IMPACT OF SEA SURFACE TEMPERATURE AND MEASUREMENT SAMPLING ON THE SMOS LEVEL 3 SALINITY PRODUCTS

Roberto Sabia[1], Alejandro Cristo[2], Marco Talone[3], Diego Fernández-Prieto[1], Marcos Portabella[3]

[1] European Space Agency, ESA – ESRIN, Frascati, Italy.
[2] University of Extremadura, Cáceres, Spain.
[3] SMOS Barcelona Expert Centre, ICM-CSIC, Barcelona, Spain.

ABSTRACT

The ESA Soil Moisture and Ocean Salinity (SMOS) mission aims at estimating, over the oceans, Sea Surface Salinity (SSS) with spatial and temporal coverage adequate for large scale oceanography. Spatio-temporal averaging of the retrieved SSS (Level 3 product) has to be properly performed in order to meet the challenging mission requirements. At high latitudes, the generally low Sea Surface Temperature (SST) characterizing the ocean degrades the brightness temperature sensitivity to SSS, but, conversely, an improvement in the Level 3 retrieved SSS performances should be expected, due to an increased pixels sampling. This trade-off between geophysical effects in cold seawater and the concomitant temporal oversampling has been addressed by analysing the latitudinal trend of the retrieved salinity performances, in various retrieval configurations and settings, once a conservative and optimal data filtering strategy is applied. Quantitative rate of changes of the SSS retrieval performance with the SST variability are provided, together with the net oversampling contribution to the L3 SSS accuracy. The experiments carried out demonstrate that the high-latitude oversampling does not compensate for the SST-driven latitudinal degradation of the L3 SSS product quality.

1. INTRODUCTION

The European Space Agency (ESA) Earth Explorer Soil Moisture and Ocean Salinity (SMOS) satellite mission is currently providing, over oceans, frequent and global estimates of Sea Surface Salinity (SSS) since its launch in November 2009 [1]. The payload onboard SMOS, the Microwave Imaging Radiometer by Aperture Synthesis (MIRAS), is a fully-polarimetric radiometer operating at the microwave frequency of 1.4 GHz (L-band), a compromise between an optimal sensitivity to SSS and a minimum perturbation from other noise sources. MIRAS provides geographically-sorted, swath-based brightness temperature (T_B) measurements (Level-1 data, L1), out of which the inversion scheme retrieves SSS [2] at 15 km sampling in a single satellite overpass (Level-2 product, L2). To meet the prescribed accuracy of the mission (0.1 psu in 100 km spatial box over a monthly period), a Level-3 (L3) product is obtained through an adequate spatio-temporal averaging of the retrieved L2 values, subsequently validated against relevant datasets [3,4].

Salinity retrieval issues whose assessment or mitigation is critical in the satellite operational data processing include: (1) improvement of T_B systematic errors estimation/removal [5]; (2) L-band Geophysical Model Function refinement [6]; (3) External noise sources characterization and removal (such as radio-frequency interference contamination, Galactic noise, Ionospheric Faraday rotation, Sun glint) [7,8].

With respect to the assessment of SMOS limitations, it has always been recognized that the influence of the Sea Surface Temperature (SST) is critical in the quality of SSS retrieval [9], since the T_B sensitivity to SSS varies from about 0.5 K/psu at 20 ºC to 0.25 K/psu at 5 ºC. This implies that the inversion performance is noticeably degraded in cold waters. However, a quantitative evaluation of this effect at latitudes exhibiting low SSTs has never been performed so far with SMOS real data. On the other hand, pixels at high latitudes are sampled more often by polar-orbiting satellites than those at low latitudes for intuitive geometrical reasons. As such, assuming that measurement errors are Gaussian, an improvement of the L3 SSS accuracy (σ) at higher latitudes should be expected as a function of the number of measurements' square root, as per Eqn 1.

$$\sigma L3_{theo} = 1/\sqrt{N} * \sigma L2 \quad (1)$$

where N is number of L2 measurements to be averaged, $\sigma L2$ is the L2 SSS accuracy and $\sigma L3_{theo}$ is the theoretical L3 SSS accuracy. Two concomitant and opposing effects are thus taking place when generating L3 products at these latitudes. A trade-off analysis between the relative impact of these two major contributions to the accuracy of the final L3 product is at the core of this study, started in a preliminary way in [10].

The overall strategy and the methodological aspects adopted are presented in Section 2. Details of the experiments performed to study how each parameter influences the

overall accuracy are discussed in Section 3. Lastly, Section 4 summarizes the main conclusions and the relevant results obtained.

2. METHODOLOGY

The concomitant influence of the SST and the oversampling in the SSS accuracy at high latitudes has been analyzed over two sample months of L2 SSS data coming from the SMOS 2012 reprocessing campaign. The main features of this study are as follows:

- Meridional transects in the South Pacific spanning from 5º to 55º S, over a 50º longitude range. The test area has been chosen in a zone mainly devoid of RFI contamination and considering only pixels in open ocean, with no land contamination.
- Sampling periods centered in the months of November 2010 and April 2011, to evaluate the various parameter influence in different seasons.
- Two different subsets of the L2 SSS v550 data (collected from the official ESA Data Processing Ground Segment) of 36 days each (as an optimal orbital sub-cycle) to ensure sampling homogeneity in the longitudinal range considered.
- L2 quality control and science flags applied to filter out data exhibiting poor geophysical retrieval and not accomplishing the minimization algorithm quality checks, in order to remove several external error sources.
- Two kinds of averaging weights considered to build L3 SSS:
  1. according to the number of L1 valid measurements used in retrieving each L2 SSS sample or
  2. taking into account the theoretical error at L2 on a pixel-base, provided by the SMOS L2 salinity processor.

To assess the latitudinal impact of SST and sampling on the quality of the L3 SSS data, the entire analysis is carried out by subdividing the test area into latitudinal bands of equal width and calculating statistics for each of them.

A substantial change adopted in [11] with regard to the previous study [10] deals with switching from a degree-based to a km-based spatial averaging box, to avoid the narrowing of the L3 boxes in longitude, thus maximizing the oversampling at high latitudes.

Besides, the potential impact of the wind speed (WS) errors and their distribution in the accuracy of the measurements needs to be taken into account to avoid distorting the interpretation of the results. This is addressed by devising a tight filtering strategy and data selection. In fact, only the L2 SSS measurements associated to a prior auxiliary WS value inside a predefined range of 6-8 m/s (where all SMOS forward models [e.g., 6] agree in the parameterization of the T_B response to WS) have been used.

Both data ensembles, arranged considering all the different L2 overpasses (36 days each, ascending passes, November 1 – December 6, 2010 and April 1 – May 6, 2011), have been divided into twenty-five latitudinal spatial bands to study, as mentioned, the meridional SSS behavior. Then, the corresponding L3 products are built by properly assigning all the measurements in a standard SMOS 100 Km×100 Km grid (Fig. 1). Each L3 SSS value is computed through a weighted average of all the L2 SSS values belonging to that box, using the weights number 1 described above (both weights identified before have proven to be similar).

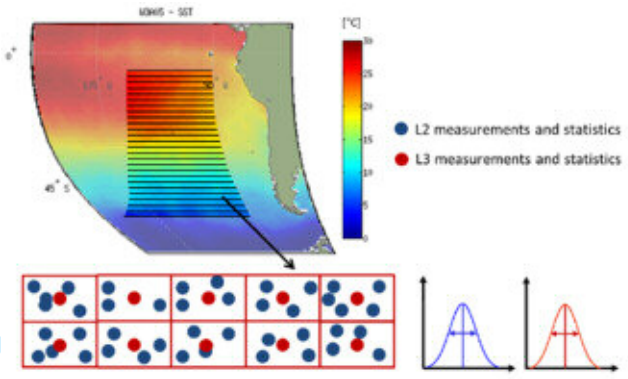

Fig. 1. Pictorial view of the L2 and L3 datasets generation and statistics computation, superimposed over a monthly mean World Ocean Atlas (WOA) 2005 SST field.

After flagging the data and once the measurements that do not fulfill the wind speed range restriction are removed, two parallel processing chains are implemented, with the objective of separating the different impacts in the SSS performance at L2 and L3.

The first dataset obtained (referred to as $L2_P$) restores the same sampling proportion of the original L2 data products, previously potentially skewed by the inhomogeneous latitudinal WS filtering. To obtain this, the L3 spatial grid (where the samples will be in a second stage averaged) is pre-defined; then, L2 measurements from each of the L3 pixels with the maximum number of L2 data are progressively randomly deleted until the desired original proportion is reached.

The second dataset (referred to as $L2_C$) has, in turn, the same number of L2 measurements for all the bands (forcing as reference the minimum number of measurements lying in the latitudinal band closest to Equator), and hence does not experience any oversampling at high latitudes. The measurement removal strategy to get this constant sampling is the same as the one for the $L2_P$. Therefore, starting from both the $L2_P$ and $L2_C$ datasets, the corresponding $L3_P$ and

$L3_C$ products are generated at Level 3. Figure 2 shows a schematic flowchart of the data filtering and processing in the chosen test area leading to the various products just mentioned.

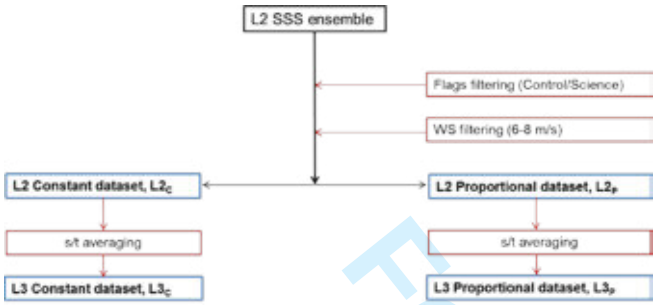

Fig. 2. Schematic diagram of the filtering strategies and the products generated for the entire test area over the studied periods.

3. RESULTS

The experiments described afterwards aim first at stressing the influence of the SST in the retrieved SSS performance when the oversampling effect is isolated, and then at deriving the relative impact of the oversampling by comparison of the L3 products obtained in the two processing chains described in the previous Section. This is performed for both temporal windows considered.

The first experiment performed, referred to the temporal window centered in November 2010, analyzes the influence of the T_B sensitivity decrease to SST changes at high latitudes. In order to do so, the standard deviation of all the L2 SSS measurements (σ_{SSS}) per each latitudinal band, i.e., over entire rows in Fig. 1, has been calculated for the $L2_C$ dataset. At this stage, only the $L2_C$ dataset has been considered (devoid of the oversampling effect), being only the effect of SST under study, thus trying to discard other possible error sources that can potentially contaminate the analysis.

In Fig. 3a, the solid blue line represents the $\sigma_{SSS\ L2}$ for the $L2_C$ dataset computed at each latitudinal band, which shows how the standard deviation increases going towards higher latitudes. The red line, in turn, represents the standard deviation of the SSS climatology (σ_{clima}) from the World Ocean Atlas (WOA) 2005, considered as the ground-truth reference [12] for the same latitudinal bands and period of the year. By properly subtracting the standard deviation of the climatological field from that of the $L2_c$ field, it is possible to decompose the latitudinal variability associated with SSS retrieval limitations (dominated by forward model sensitivities to the different geophysical parameters) from the expected natural variability of the field itself (using WOA as truth). To this end, the quadratic difference between the $\sigma_{SSS\ L2}$ and σ_{clima} is computed, and the resulting black curve ($\sigma_{net\ L2}$) is meant to represent the influence of SST on the SSS variability, once that the WS influence has been previously isolated, as discussed. Note however that additional residual influence of SMOS external noise sources (such as Galactic noise, RFI, Sun contamination etc) cannot be excluded, but both the choice of the test area (coincident with the zone chosen by the SMOS community to perform the satellite bias mitigation over the oceans) and the configuration and flagging strategies adopted ensure that the SST is the paramount driver of the latitudinal variability shown.

This $\sigma_{net\ L2}$ is also plotted as black solid line against the mean SST per latitudinal band, as shown in Fig. 3b. It can be noted that high $\sigma_{net\ L2}$ values are in correspondence of low SSTs, in accordance to the challenging SSS retrieval experienced in cold waters. Moreover, both a linear fit (solid yellow line) and a quadratic fit (dashed yellow line) are represented. The linear fit quantifies the incremental error that should be expected in the L2 product as a function of SST (Eqn. 2), whose slope is:

$$\Delta \sigma_{L2} / \Delta \mathrm{SST} = -0.05 \text{ psu/°C} \qquad (2)$$

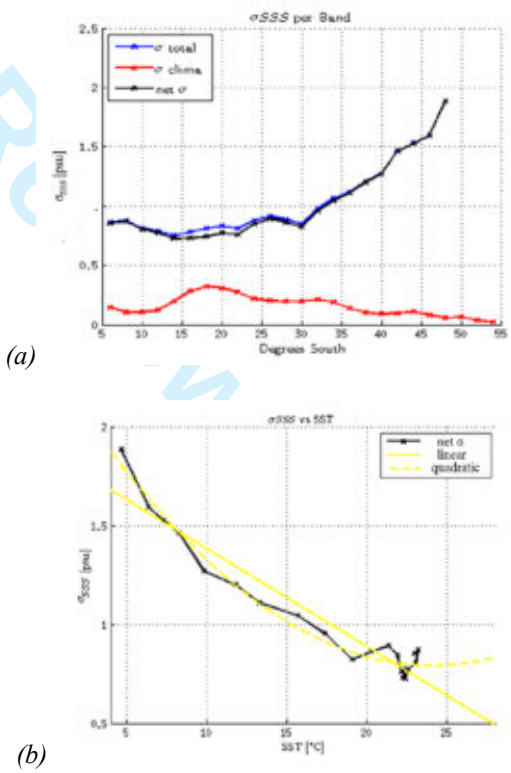

Fig. 3. Effect of the T_B sensitivity degradation with respect to (a) the different bands for the $L2_C$ dataset. (b) the SST for the $L2_C$ dataset.

The second experiment (again referring to the first 36-day subset) aims at assessing the relative effect of the oversampling on the retrieval performance at L3. The two datasets $L2_P$ and $L2_C$ are projected up to L3 ($L3_P$ and $L3_C$, labeled as "proportional" and "constant" in the figures), as it is shown in Fig. 4a, in which they are plotted (as a solid and dashed black line, respectively) together with the corresponding climatology (in red) and the mean SST per band (in green). As said, the $L3_C$ dataset has been arranged with the same number of L2 measurements per band and it does not experience the oversampling influence. In contrast, the $L3_P$ dataset does include the oversampling. As expected, the $L3_P$ curve generally lays below the $L3_C$, since the oversampling obviously results in a reduction of the standard deviation values. Therefore, an estimation of how much the oversampling affects the accuracy of the L3 data product can be performed by comparison. To highlight this, the climatology variability has been again subtracted quadratically from the $\sigma_{SSS\ L3}$ of both L3 datasets. Then, the corresponding $\sigma_{net\ L3p}$ and $\sigma_{net\ L3c}$ curves have been plotted in Fig. 4b as black solid and dashed lines, respectively. The difference between the two curves (in magenta) therefore shows the latitudinal variation of error reduction that it is related to the oversampling effect.

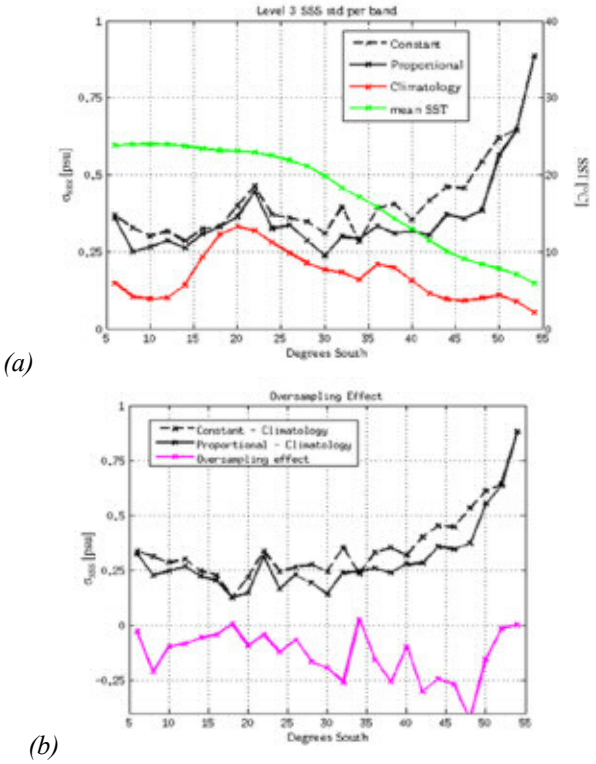

Fig. 4. Effects of the oversampling contribution; a) $\sigma_{SSS\ L3}$ for both $L3_P$ and $L3_C$ datasets compared with climatology and SST and b) $\sigma_{net\ L3}$ for both datasets with the their corresponding difference

To test the robustness of the study and check for inter-seasonal effects, the same analysis has been performed over another temporal window of 36 days, 6 months apart (April 1 – May 6, 2011).

The equivalent of the Fig. 3a,b are not shown since the behavior is consistent and major conclusions hold. Also, the linear fit of the $\sigma_{net\ L2}$ against the SST has almost exactly the same slope of the previous one, stressing how the accuracy worsening related to SST changes consistently with the latitude at the indicated rate of the Eqn. 1.

Figures 5 show the same curves as in Fig. 4, where the L3 analysis is reported, but for the new dataset period. In Fig. 5a, the black curves are flatter than those in Fig. 4, and the SST on average higher. On the other hand, when climatology standard deviation is quadratically subtracted, the resulting $\sigma_{net\ L3}$ curves in Fig. 5b show an increasing trend at high latitudes, as evidenced before in Fig. 4b. The magenta line in Fig 5b, indicating the relative net contribution of the oversampling, is also consistent with that of Fig. 4b for the month of November 2010, since the slight negative latitudinal slope (indicating that the oversampling is more efficient at higher latitudes) is kept.

Both experiments showed a quantitative latitudinal estimation of the influences of the parameters at stake, clearly demonstrating that the much higher influence of the SST in the SSS performance is not compensated by the error reduction due to the oversampling at high latitudes.

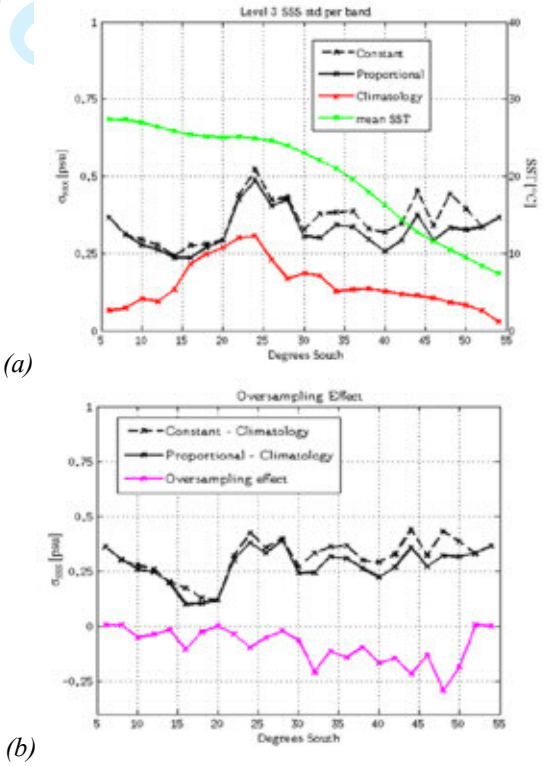

Fig. 5. Same as Fig.4, for the month of April 2011.

4. CONCLUSIONS

In this study, the latitudinal influence of both the T_B sensitivity to SST changes and the measurement sampling is analyzed in terms of L2 and L3 SSS products accuracy.

This has been addressed by generating pairs of L2 and L3 datasets over two sample months under specific configurations and settings, and adopting proper data flagging/filtering strategy (especially isolating potential contamination due to WS).

The emphasis is put on the quantitative estimates of the σ_{L2} increase with latitude that can be attributed to the T_B sensitivity decrease to SST changes, and on the net oversampling contribution to the L3 accuracy. As a matter of fact, the high-latitude oversampling does not compensate for the SST-driven latitudinal degradation of the L3 SSS product quality.

By looking at L3 quantitative performance, the computed SSS accuracy is noticeably worse than that predicted by theory (Eqn. 1), due to spatial correlation patterns which render averaging error reduction poorly efficient. No further SMOS contaminations are isolated (such as RFI, Galactic noise, etc), and their effect in this quantitative evaluation cannot be excluded. However, by looking at different periods of time, it is concluded that the latitudinal pattern persists despite these effects.

Eventually, this analysis shows that the T_B degraded sensitivity in cold waters translates into a remarkable worsening of the SSS retrieval performances, and this can be a burden for the salinity estimation at mid-high latitudes, where several paramount oceanographic processes take place.

5. REFERENCES

[1] Mecklenburg, S.; Drusch, M.; Kerr, Y.H.; Font, J.; Martin-Neira, M.; Delwart, S.; Buenadicha, G.; Reul, N.; Daganzo-Eusebio, E.; Oliva, R.; Crapolicchio, R., "ESA's Soil Moisture and Ocean Salinity Mission: Mission Performance and Operations," Geoscience and Remote Sensing, IEEE Transactions on , vol.50, no.5, pp.1354,1366, May 2012, doi: 10.1109/TGRS.2012.2187666

[2] Zine, S.; Boutin, J.; Font, J.; Reul, N.; Waldteufel, P.; Gabarro, C.; Tenerelli, J.; Petitcolin, F.; Vergely, J.-L.; Talone, M.; Delwart, S., "Overview of the SMOS Sea Surface Salinity Prototype Processor," Geoscience and Remote Sensing, IEEE Transactions on , vol.46, no.3, pp.621,645, March 2008, doi: 10.1109/TGRS.2008.915543.

[3] Boutin, J.; Martin, N.; Xiaobin Yin; Font, J.; Reul, N.; Spurgeon, P., "First Assessment of SMOS Data Over Open Ocean: Part II—Sea Surface Salinity," Geoscience and Remote Sensing, IEEE Transactions on , vol.50, no.5, pp.1662,1675, May 2012, doi: 10.1109/TGRS.2012.218454.

[4] Banks, C.J.; Gommenginger, C.P.; Srokosz, M.A.; Snaith, H.M., "Validating SMOS Ocean Surface Salinity in the Atlantic With Argo and Operational Ocean Model Data," Geoscience and Remote Sensing, IEEE Transactions on , vol.50, no.5, pp.1688,1702, May 2012, doi: 10.1109/TGRS.2011.2167340.

[5] Gourrion, J.; Guimbard, S.; Portabella, M.; Sabia, R., "Toward an Optimal Estimation of the SMOS Antenna-Frame Systematic Errors," Geoscience and Remote Sensing, IEEE Transactions on, vol.51, no.9, pp.4752,4760, 2013.

[6] Guimbard, S.; Gourrion, J.; Portabella, M.; Turiel, A.; Gabarro, C.; Font, J., "SMOS Semi-Empirical Ocean Forward Model Adjustment," Geoscience and Remote Sensing, IEEE Transactions on , vol.50, no.5, pp.1676,1687, May 2012, doi: 10.1109/TGRS.2012.2188410.

[7] Font, J. et al., : SMOS first data analysis for sea surface salinity determination, International Journal of Remote Sensing, Vol. 34, Iss. 9-10, 2013.

[8] Reul, N.; Tenerelli, J.; Boutin, J.; Chapron, B.; Paul, F.; Brion, E.; Gaillard, F.; Archer, O., "Overview of the First SMOS Sea Surface Salinity Products. Part I: Quality Assessment for the Second Half of 2010," Geoscience and Remote Sensing, IEEE Transactions on , vol.50, no.5, pp.1636,1647, May 2012.

[9] Font, J., A. Camps, A. Borges, M. Martín-Neira, J. Boutin, N. Reul, Y. H. Kerr, A. Hahne, and S. Mecklenburg, "SMOS: The challenging sea surface salinity measurement from space," Proc. IEEE, vol. 98, 649-665, 2010.

[10] Sabia, R., M. Talone, M. Portabella, D. Fernández-Prieto, J. Gourrion, A. Camps and J. Font, "SMOS L3 Salinity Performances at Decreasing Sea Surface Temperature", Proceedings of MicroRad 2012, Rome, Italy, 5-9 March 2012.

[11] Cristo, A., R. Sabia, M. Talone, D. Fernández-Prieto, M. Portabella; Geophysical Effects at Increasing Latitudes in the SMOS L3 Salinity Products; Proceedings of the IEEE GOLD Remote Sensing Conference 2012, Roma, Italy, June 4-5, 2012, ISBN13: 978-88-7431-668-7, Giannini Ed.

[12] Antonov, J. I., R. A. Locarnini, T. P. Boyer, A. V. Mishonov, and H. E. Garcia, 2006. World Ocean Atlas 2005, Volume 2: Salinity. S. Levitus, Ed. NOAA Atlas NESDIS 62, U.S. Government Printing Office, Washington, D.C., 182 pp.